SUPPORTING INFORMATION

Super-Resolution Fluorescence of Huntingtin Reveals Growth of Globular Species into Short Fibers and Coexistence of Distinct Aggregates

Whitney C. Duim,[†,‡,*] Yan Jiang,[†,§,‡] Koning Shen,[‖] Judith Frydman,[‖] and W. E. Moerner[†]

[†]Department of Chemistry, [§]Department of Applied Physics, and [‖]Department of Biology, Stanford University, Stanford, CA 94305, USA
[‡]Present addresses: Department of Biological Sciences, University of Southern California, Los Angeles, CA 90089, USA (W. C. D.) and Program in Cellular and Molecular Medicine, Boston Children's Hospital, Boston, MA 02215, USA (Y. J.)

*Corresponding author: wduim@usc.edu

Single-Molecule Counting of Cy3-Labeled Htt-ex1

To characterize the early stages of Htt-ex1 aggregation, we aimed to count the number of Htt-ex1 monomers in small Htt-ex1 aggregates.[1, 2] MBP-Htt-ex1 was labeled with the counting dye Cy3 maleimide[3, 4] (GE Healthcare), aggregation reactions of only MBP-Htt-ex1-Cy3 were set up as described in the Methods, and aliquots were removed at several time points. The aliquots were diluted to 100 pM and adsorbed to clean glass coverslips (with and without poly-L-lysine coatings) for imaging. The number of Cy3 fluorophores (and thus the number of Htt-ex1 proteins) in the aggregates were counted through observation of the number of photobleaching steps. Figure S2a shows a typical photobleaching intensity trace extracted from the imaging. Histograms of the step numbers (Figure S2b) revealed a predominance of monomers, dimers, and trimers even at long aggregation times such as 24 hours. There were several possible reasons for this: (1) dilution of the sample before imaging disrupted small soluble aggregates, (2) the covalently-attached Cy3 fluorophores altered the aggregation process, and (3) initial nucleation was a sufficiently rare event such that the population of larger oligomers was difficult to observe. We found compelling evidence for the results of our experiment from reasons (2) and (3).

The initial ensemble-level characterization of the aggregation reaction by filter trap assay [5, 6] showed the Htt-ex1 and Htt-ex1-Cy3 aggregation reactions to be identical (Figure S2c,d). However, the appearances of the aggregates as examined by phase contrast, fluorescence microscopy, and AFM at 5 and 24 hours were quite different (Figure S2e,f). The species observed when an Htt-ex1-Cy3-only aggregation reaction was adsorbed to a coverslip were a very small number of very large aggregates. Most of the coverslip surface was empty, while in contrast the surface was littered with fibers for unlabeled Htt-ex1 aggregation. However, aggregation of mixtures of Htt-ex1 and Htt-ex1-Cy3 at ratios greater than 10:1 appeared "normal." This same phenomenon was observed with every dye we labeled the Htt-ex1 with (Cy3, ATTO 655,[7] Alexa Fluor 647), although the morphologies of the abnormal aggregates differed. We hypothesized that the fluorescent dye molecules were large enough to disrupt the contacts made between Htt-ex1 monomers during aggregation, limiting the number of aggregates that were able to form and sending the aggregates that did form down a different aggregation pathway (thus producing different morphologies).

Imaging of un-diluted aggregation reactions showed that the population of monomers and small oligomers was much greater (estimated 10^7 times larger) than the population of large fibrillar aggregates (see the "carpet" of fluorescent monomers in Figure 2 and small species around the fibers in Figure S5). We concluded that the initial nucleation and oligomerization were such rare events that only a small fraction of Htt-ex1 entered the aggregation pathway to form large fibers (reason 3). In the single-molecule imaging of diluted aggregation reactions, we detected only the very large population of monomers and small oligomers. Therefore, we turned to studying the Htt-ex1 aggregate species at bulk micromolar concentrations.

Factor Xa Cleavage of MBP-Htt-ex1-Alexa 647

We confirmed that the Alexa 647 (AX647) dye did not interfere with Factor Xa cleavage of the MBP-Htt-ex1-AX647. The cleavage of MBP-Htt-ex1-AX647 labeled at a dye to protein ratio of 0.68 was compared to unlabeled MBP-Htt-ex1 using SDS-PAGE with fluorescence imaging and Coomassie staining. Aliquots removed from the aggregation reactions at defined time points were boiled with SDS loading buffer to stop the aggregation reaction[5] and prepare the sample to be loaded for PAGE on a 12% gel. The gels were first imaged on a Typhoon 9410 scanner (GE Healthcare) with 633 nm laser excitation and 670BP30 emission collection, and then stained with Coomassie. The results (Figure S3) indicated that the labeled and unlabeled proteins were cleaved from the MBP with similar efficiency by Factor Xa.

Fluorophore Selection

In our initial super-resolution (SR) imaging of Htt-ex1 aggregates,[7] we utilized ATTO 655 maleimide conjugated to Htt-ex1 monomers based on reports of the excellent (and tunable) blinking behavior of the dye in the presence of reducing and oxidizing agents.[8-11] The dye Alexa Fluor 647 has been shown to reversibly switch from an emissive to a long-lived dark state (blink) through the reaction of added primary thiol reagents with the fluorophore under red laser excitation.[12] The dye has performed very well in a number of demanding SR experiments including the mapping of synaptic proteins,[13] imaging of Alzheimer's disease β-amyloid aggregates,[14] and 3D double-helix point spread function imaging of microtubules in fixed mammalian cells.[15] Further, in the Zhuang group's evaluation of 26 commercial dyes with thiol and oxygen scavenger additives, AX647 emerged as the best dye for SR applications.[16] Among other advantages, AX647 emits many more photons per switching event than ATTO 655. The

localization precision attainable scales primarily as $1/\sqrt{N}$, where N is the number of detected photons. Thus, to increase the resolution of our fluorescence images of Htt-ex1 aggregates, we switched fluorophores from ATTO 655 to AX647.

Ratio of Labeled Htt-ex1 in Aggregates

The ratio of Htt-ex1 to Htt-ex1-AX647 used in the experiments was chosen by comparison of phase contrast and AFM images of the aggregates at different ratios to images of unlabeled Htt-ex1 aggregates. We found that bulk-level quantitative measures, such as filter trap assays, could be misleading. For example, the filter trap results for unlabeled Htt-ex1 and 82%-labeled Htt-ex1-Cy3 were comparable (Figure S2c,d), while the morphologies of the aggregates as examined by phase contrast (Figure S2e,f) and AFM were markedly different. Figures S4 and S5 show phase contrast and high-resolution AFM images, respectively, of the Htt-ex1:Htt-ex1-AX647 = 10:1 aggregates. We employed the quantitative techniques of Thioflavin T fluorescence and attenuance (Figure S6) to corroborate our ratio selection.

Ensemble Measurements of Htt-ex1 Aggregation Over Time

The Thioflavin T (ThT) and attenuance measurements of Htt-ex1 aggregation were performed in 96-well plates (Corning) with a plate reader (Tecan Infinite M1000). The fluorescence of each well containing 12.5 μM ThT was recorded every 15 minutes with 446 nm excitation and 490 nm emission (5 nm bandwidths). Because the AX647 dye would have interfered spectrally with the ThT assay and the formation of insoluble protein aggregates increases the turbidity of a sample, the attenuance, or absorbance of the sample due to scattering or reflection, was measured.[17, 18] Attenuance was measured instead of right-angle light scattering because of the geometrical constraints of the plate reader. The protocol for attenuance was nearly the same as for ThT, except that no ThT was added and the absorbance at 340 nm (or 405 nm) was measured.

Figure S6a shows the expected sigmoidal curve of ThT fluorescence as β-sheet-structured Htt-ex1 aggregates were formed following Factor Xa cleavage.[19-22] To compare the aggregation kinetics of Htt-ex1:Htt-ex1-AX647 = 10:1 to Htt-ex1-only, the attenuance was measured at 340 nm and 405 nm. The attenuance curves (which were very similar for 340 and 405 nm) were corrected by the attenuance of buffer. The corrected attenuance values of duplicate Htt-ex1:Htt-ex1-AX647 = 10:1 + Factor Xa samples were larger than the duplicate Htt-ex1 + Factor Xa

values. In Figure S6b, the Htt-ex1 and Htt-ex1:Htt-ex1-AX647 = 10:1 + Factor Xa curves, and – Factor Xa curves, are overlaid for direct comparison of the kinetics.

Both the ThT and attenuance data in Figure S6 indicate slow aggregation between 0 and approximately 5 hours (the nucleation/oligomerization period) followed by rapid aggregate growth through approximately hour 15. Aggregate growth then slows and new ThT binding sites cease to be created after 30 hours. The attenuance signal, however, continues to increase, which agrees with our hypothesis that existing aggregate fibers assemble into even larger aggregates (with larger scattering cross-sections) at long incubation times.

Characterization of AX647 as a Label of Htt-ex1 under Blinking Conditions

A time trace of the single-molecule AX647's blinking behavior is shown in Figure S7a. As described in a recent report,[16] the low on-off duty cycle ($t_{on}/[t_{on} + t_{off}]$) and high photon count per emissive event make AX647 an ideal fluorophore for SR imaging. Typically, we detected 1000-5000 photons per single molecule per frame (7.5 ms frame^{-1}). Figure S7b displays a representative histogram of photon counts for fluorophores localized by the SR algorithm.

The localization precision was computed in three different ways by (1) the equation for the theoretical precision of localization,[23] (2) the distribution of positions of repeatedly localized single molecules,[24] and (3) the statistical 95% confidence interval of the center of the 2D Gaussian fit to each single-molecule point-spread function (PSF).[7, 25] The theoretical localization precision was calculated, with the parameters extracted from the Gaussian fits to the single-molecule PSFs, as

$$\sigma = \sqrt{\frac{s^2 + a^2/12}{N} + \frac{8\pi s^4 b^2}{a^2 N^2}}$$

where s is the standard deviation of the Gaussian fit to the PSF, a is the pixel size, b is the background noise, and N is the number of photons collected.[23] The average background noise measured directly from the frames of the movies was 9 photons pixel^{-1}, yielding average theoretical localization precisions of around 4 nm.

Single molecules that appeared in many frames with little blinking behavior and that were spatially separated from neighboring molecules were repeatedly localized to provide an

experimental measure of the localization precision. Although such a measurement is not always possible, it provides a more realistic estimate since the distribution of localizations is directly measured without an assumed theoretical model of background and pixilation contributions to Poisson statistics. Figure S8a and b show the results from the localization of one such molecule over the course of more than 1,000 frames (7.5 s). The localization precisions in x and y are given by the standard deviations of the distributions: σ_x = 7.8 nm and σ_y = 9.2 nm.

In our fitting algorithm, we have characterized the uncertainty in the center coordinate of the 2D Gaussian fit with a statistical 95% confidence interval. We have also defined the localization precision as half of the statistical 95% confidence interval.[7, 25] Figure S8c is a histogram of the localization precisions as just defined for the fit distributions in Figure S8a and b. As expected, the mean value of 12.7 nm is a more conservative value for the resolution limit of the fits than the theoretical value or the value obtained from repetitive localizations.

Htt-ex1 Seed Growth

The ratio of the concentration of Htt-ex1 added to the concentration of the starting seeds (changed by seed dilution) affected the length of fibers grown. At no dilution of the seeds, the fibers were ~ 200 nm in length (Figure S9a). At seed dilutions of five- and ten-fold, the lengths of the fibers increased to the 500 nm to 1 μm range (Figure S9b, d). It is also of note that the growth of the seeds into fibers was fast compared to the growth of fibers from monomers. We did not quantify this in detail, but AFM images taken of a sample at 5 hours and 24 hours were virtually indistinguishable. This result supports the nucleated growth model of Htt-ex1 and agrees with the accelerated growth curves observed for bulk seeded Htt-ex1 aggregation reactions.[21]

```
        10          20          30          40          50          60
MKIKTGARIL ALSALTTMMF SASALAKIEE GKLVIWINGD KGYNGLAEVG KKFEKDTGIK

        70          80          90         100         110         120
VTVEHPDKLE EKFPQVAATG DGPDIIFWAH DRFGGYAQSG LLAEITPDKA FQDKLYPFTW

       130         140         150         160         170         180
DAVRYNGKLI AYPIAVEALS LIYNKDLLPN PPKTWEEIPA LDKELKAKGK SALMFNLQEP

       190         200         210         220         230         240
YFTWPLIAAD GGYAFKYENG KYDIKDVGVD NAGAKAGLTF LVDLIKNKHM NADTDYSIAE

       250         260         270         280         290         300
AAFNKGETAM TINGPWAWSN IDTSKVNYGV TVLPTFKGQP SKPFVGVLSA GINAASPNKE

       310         320         330         340         350         360
LAKEFLENYL LTDEGLEAVN KDKPLGAVAL KSYEEELAKD PRIAATMENA QKGEIMPNIP

       370         380         390         400         410         420
QMSAFWYAVR TAVINAASGR QTVDEALKDA QTNSSSNNNN NNNNNNLGIE GRISEFGSMS

       430         440         450         460         470         480
TGGGMATLEK LMKAFESLKS FQQQQQQQQQ QQQQQQQQQQ QQQQQQQQQQ QQQQQQQQQQ

       490         500         510         520         530         540
QQQQQPPPPP PPPPPPQLPQ PPPQAQPLLP QPQPPPPPPP PPPGPAVAEE PLHRPCGSHH

HHHH
```

Figure S1. Amino acid sequence of MBP-HttQ44-exon1-S112C-histag. The MBP sequence is followed by a linker region containing the Factor Xa cleavage site (bold red). The Htt-exon1 sequence is shaded in gray and position S112C of exon1 is underlined.

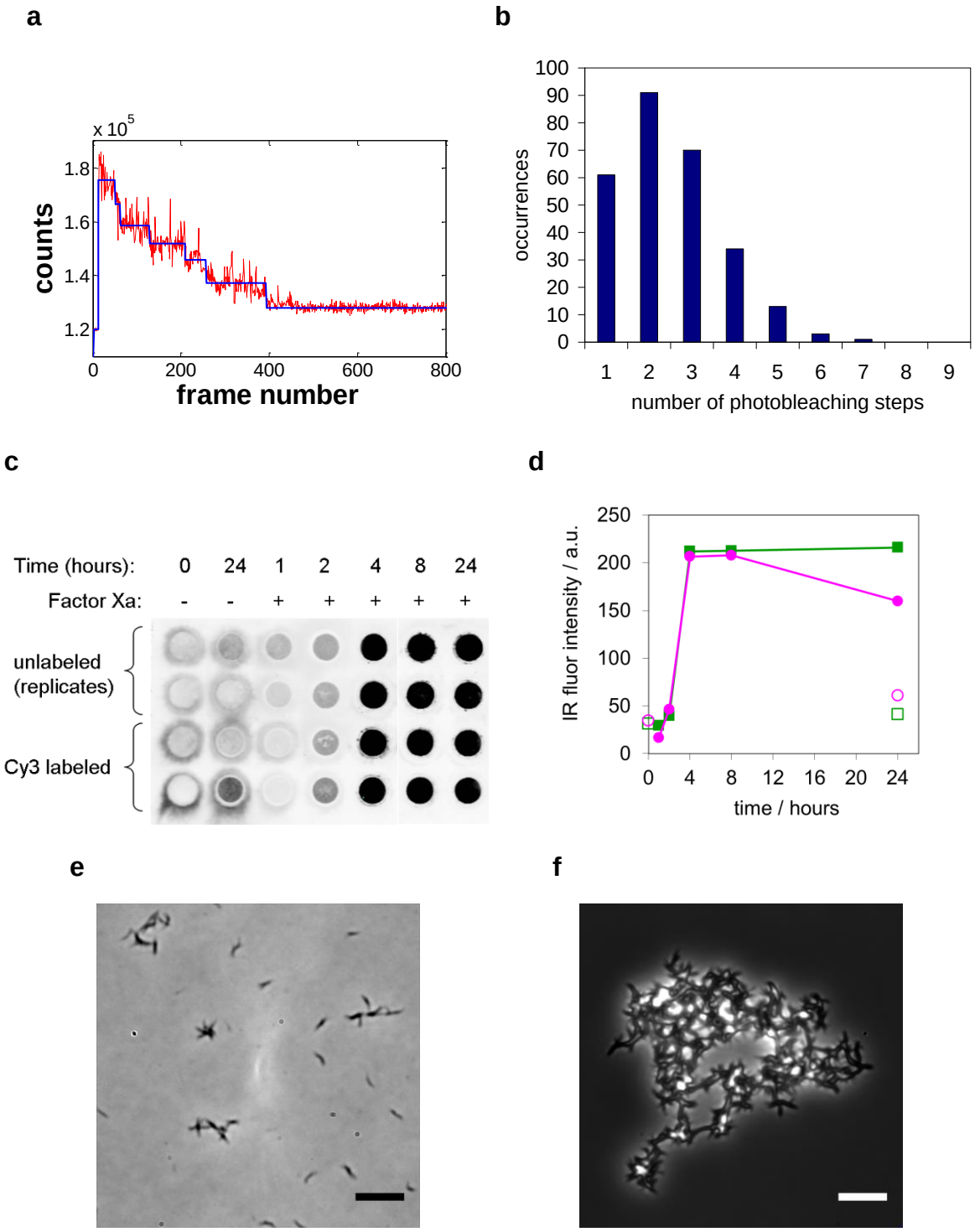

Figure S2. Aggregation of Cy3-labeled Htt-ex1. a) Htt-ex1-Cy3 after 4.5 hours of aggregation was imaged at 100 pM on a poly-L-lysine-coated glass slide with 532 nm excitation. The MBP-Htt-ex1-Cy3 used here was 82% labeled. The intensity trace of a Htt-ex1-Cy3 oligomer photobleaching was obtained at 50 ms exposure and the vertical blue lines mark the change points that were calculated using Watkins' and Yang's method.[4, 26] b) Histogram of the number

of steps (fluorophores) for 273 spots from the experiment in a) indicating that the majority of the population was small oligomers (mean = 2.5). c) Filter trap data where the gray to dark black circles on the filter membrane indicate an increasing amount of Htt-ex1 aggregates larger than the 200 nm membrane pore size. Detection on a Li-Cor Odyssey scanner was via antibody against his-tag (monoclonal anti-his antibody conjugated to biotin, GenScript Corp.) and IRDye 800CW streptavidin-conjugate (Li-Cor Biosciences).[6] d) The fluorescence intensity of the circles in c) over time is plotted. The intensities of the unlabeled (green squares) and labeled (pink circles) Htt-ex1 are nearly identical over the 24 hour sampling period. As expected, little signal is observed for the uncleaved MBP-Htt-ex1 (open green squares) or MBP-Htt-ex1-Cy3 (open pink circles) at 0 and 24 hours. Phase contrast images of e) Htt-ex1 and f) Htt-ex1-Cy3 (75% labeled stock) aggregates 24 hours after Factor Xa addition. The Htt-ex1 fibers in e) represent normal Htt-ex1 aggregation. The large Htt-ex1-Cy3 aggregate in f) is fluorescent when excited at 532 nm. The scale bars are 5 μm and different contrasts are used to display the two images.

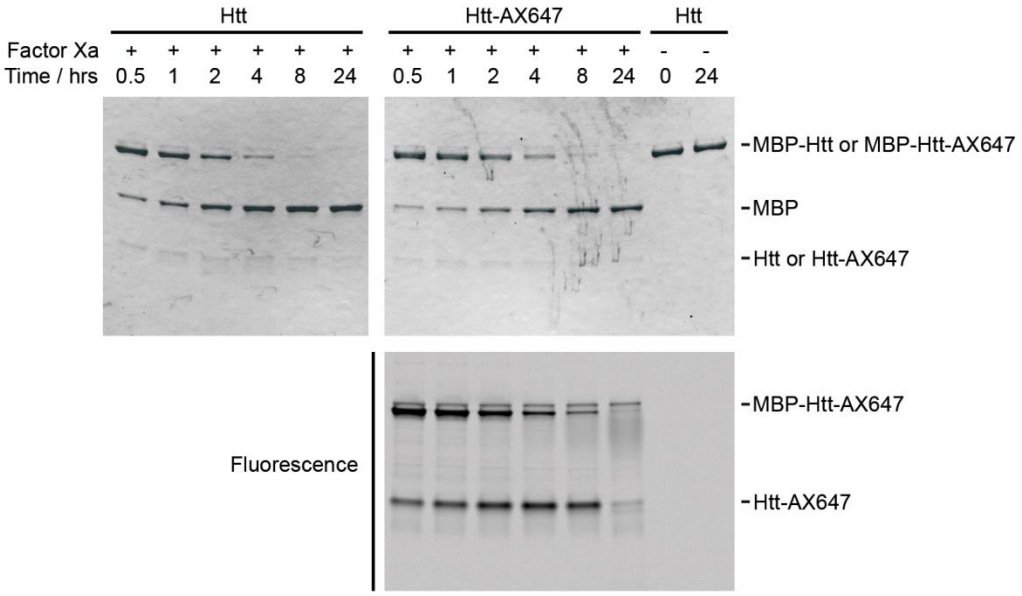

Figure S3. Factor Xa cleavage of Htt-ex1 protein monitored by SDS-PAGE. MBP-Htt-ex1 and 68% labeled MBP-Htt-ex1-AX647 were cleaved with similar efficiency by Factor Xa. The protein was visualized by Coomassie staining (top row) and fluorescence (bottom row). Note that the reduced signal of the Htt-AX647 in the 24-hours lane was due to aggregation of the construct: large aggregates were unable to enter the gel and appeared as fluorescence signal in the wells at the top of the gel.

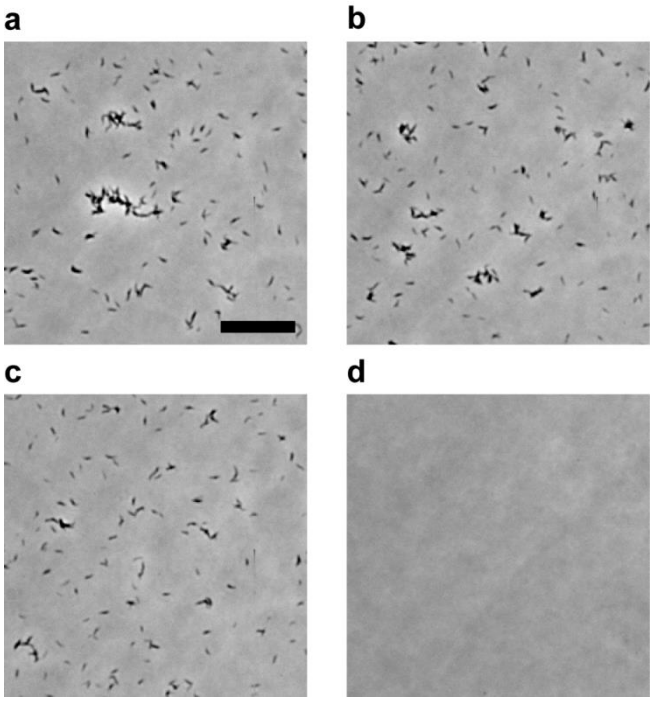

Figure S4. Phase contrast survey images of Htt-ex1:Htt-ex1-AX647 = 10:1 after 24 hours. Htt-ex1 aggregates appeared as a range of fibers and fiber assemblies (a-c). If Factor Xa was omitted from the mixture, no aggregate species were observed at 24 hours (d). Scale bar of 10 μm applies to all panels. All images are presented at the same contrast level.

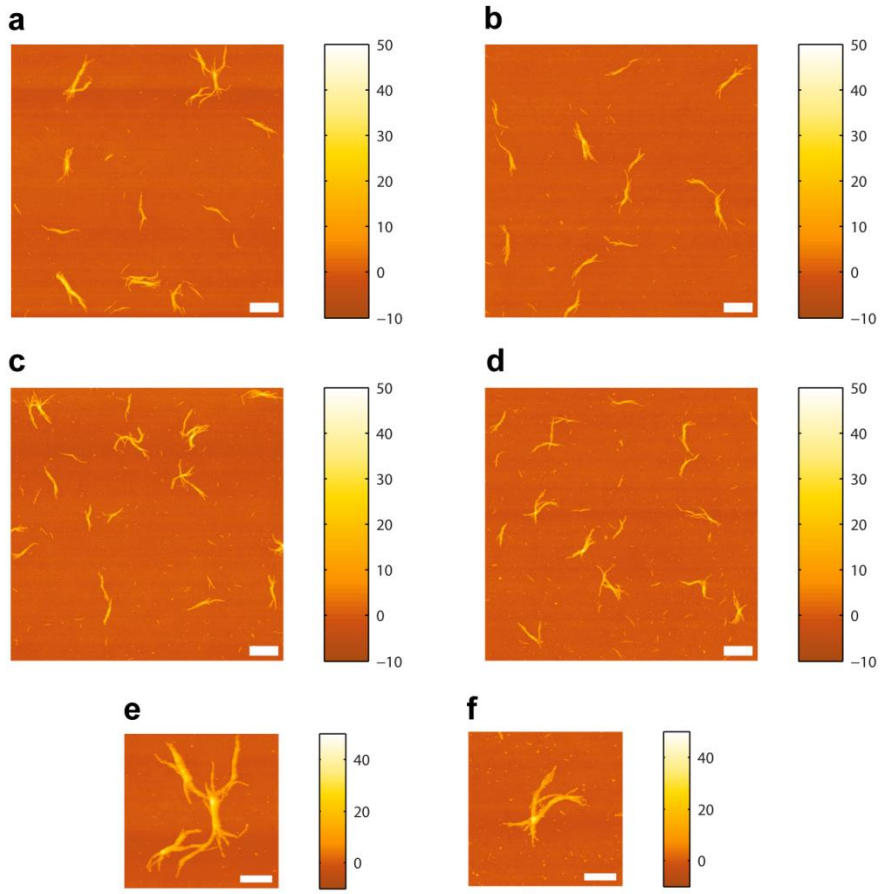

Figure S5. AFM topography maps of Htt-ex1 fibers after 24 hours of aggregation. The aggregates formed from a)-b) Htt-ex1 only and c)-d) Htt-ex1:Htt-ex1-AX647 = 10:1 have equivalent morphologies. Magnified views of the fibrous, broom-like aggregates from a) and d) are displayed in e) and f). The colorbars indicate the z-height in nm and the image resolution is 9.8 nm pixel^{-1}. Scale bars a)-d) = 1 µm and e)-f) = 500 nm.

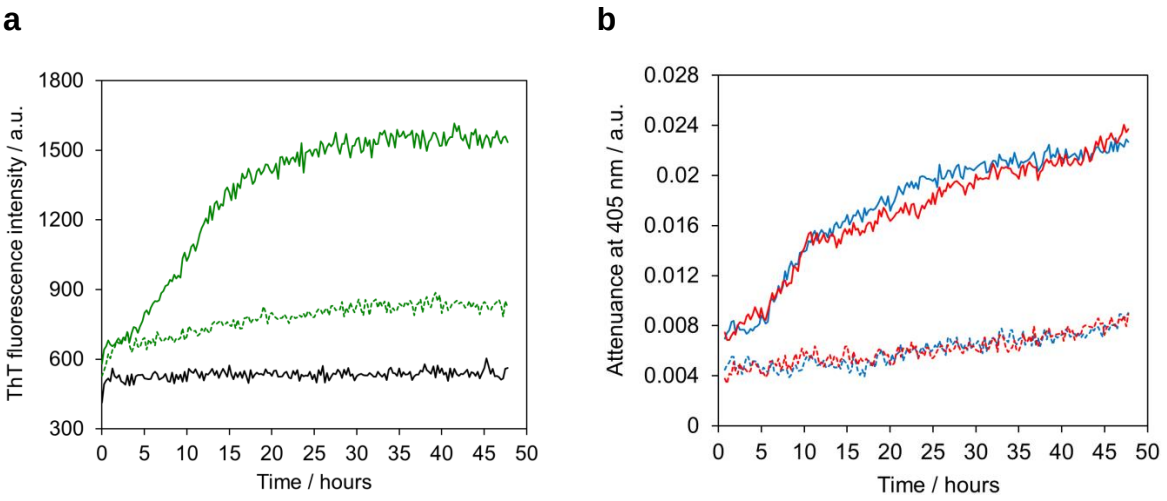

Figure S6. Bulk assays of Htt-ex1 aggregation. a) Kinetics of Htt-ex1 aggregation as monitored by ThT binding. The curves are Htt-ex1 + Factor Xa (solid green), Htt-ex1 – Factor Xa (dashed green), and buffer (solid black). b) Attenuance of aggregation reactions over time: Htt-ex1 + Factor Xa (solid blue), Htt-ex1:Htt-ex1-AX647 = 10:1 + Factor Xa (solid red), Htt-ex1 – Factor Xa (dashed blue), and Htt-ex1:Htt-ex1-AX647 = 10:1 – Factor Xa (dashed red). The data is overlaid for comparison. The points before 45 minutes are not plotted because all four replicates of the buffer sample showed fluctuations in attenuance that were large in magnitude compared to the fluctuations in the signal over the rest of the experiment. The fluctuations may have been the result of short-lived bubbles in the buffer or initial instrument instability.

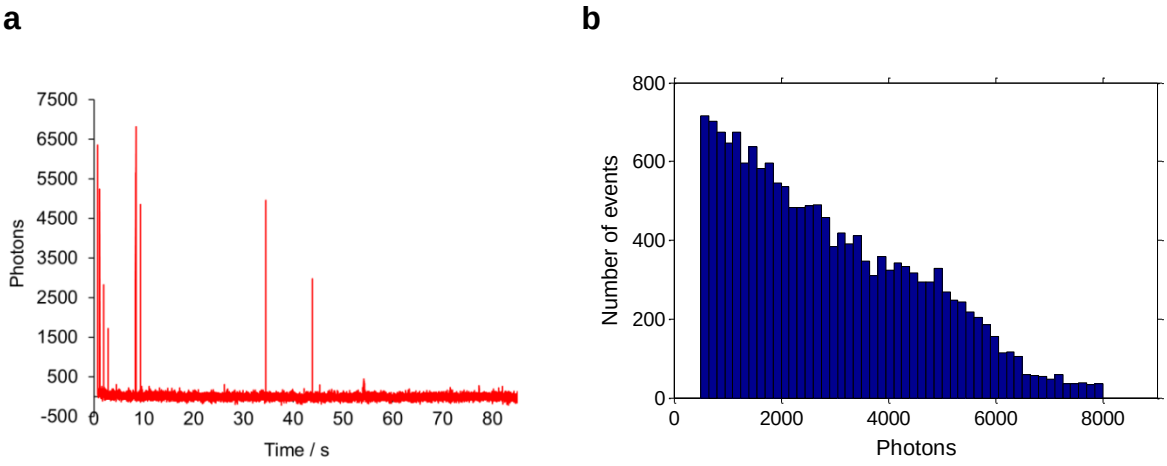

Figure S7. Characterization of the photon emission of AX647. a) Time trace of a single AX647 fluorophore covalently attached to Htt-ex1 under blinking conditions. Each frame was 7.5 ms. The sample was prepared by adsorbing a 46 hour-old aggregation reaction of 4.2 µM Htt-ex1 to glass to which 1 nM Htt-ex1-AX647 had been added at the 6-hour mark and adding blink buffer. b) Histogram of photons detected above background per single molecule per frame from a collection of 16-hour Htt-ex1:Htt-ex1-AX647 = 10:1 aggregates. The median value was 2,560 photons. The data shown had been thresholded first, as is visible from the data range of 500 to 8,000 photons.

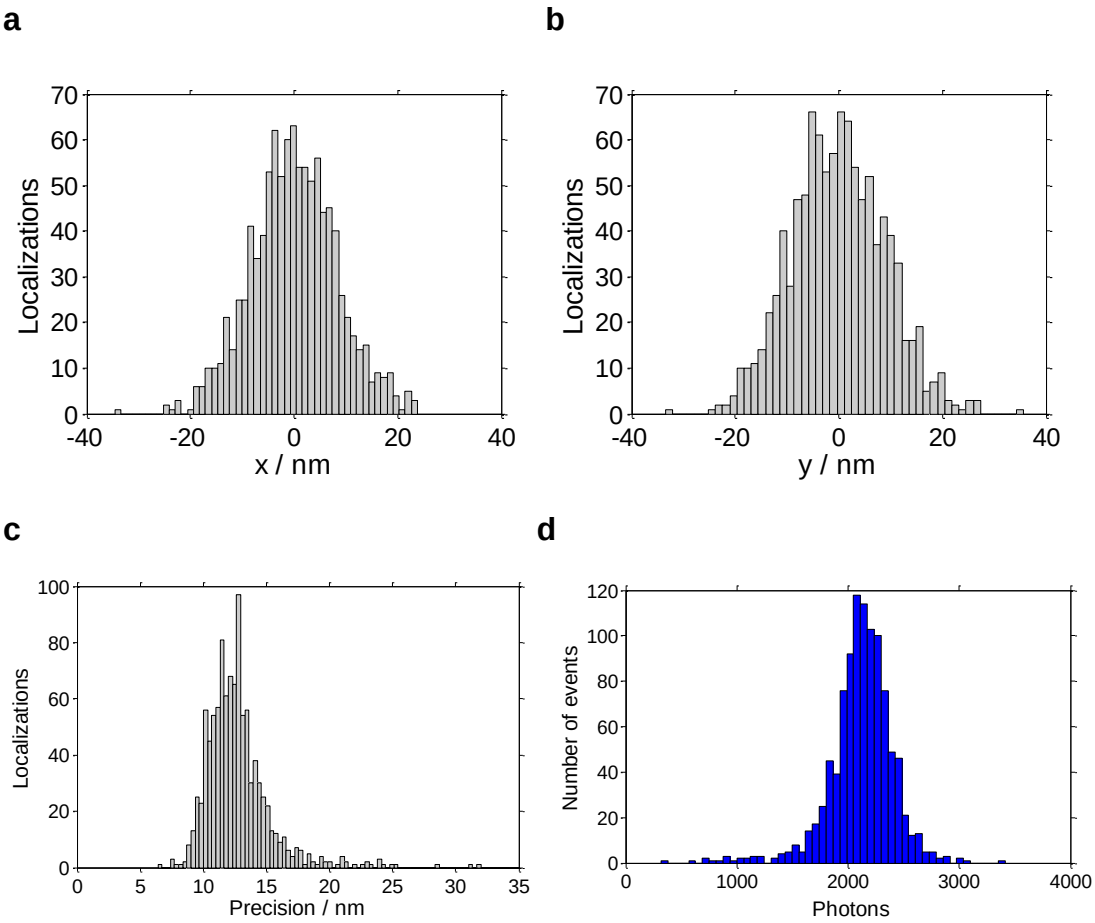

Figure S8. Comparison of experimental and statistical localization precisions for an individual molecule of AX647. The molecule was localized 1,023 times. The histograms of the a) x and b) y coordinates of the localizations were fit by Gaussian functions with standard deviations of σ_x = 7.8 nm and σ_y = 9.2 nm. c) Distribution of the statistical localization precisions given by half of the 95% confidence interval of the fits with a mean value of 12.7 nm (in x and y). d) Histogram of photon counts per localization (mean = 2,118 photons). The distribution here is quite different from Figure S7b. The distribution in Figure S7b includes thousands of molecules in different microenvironments and locations on the glass slide with respect to the Gaussian-profile excitation beam, which likely affected the photon counts per frame. In contrast, the distribution here is of one molecule only.

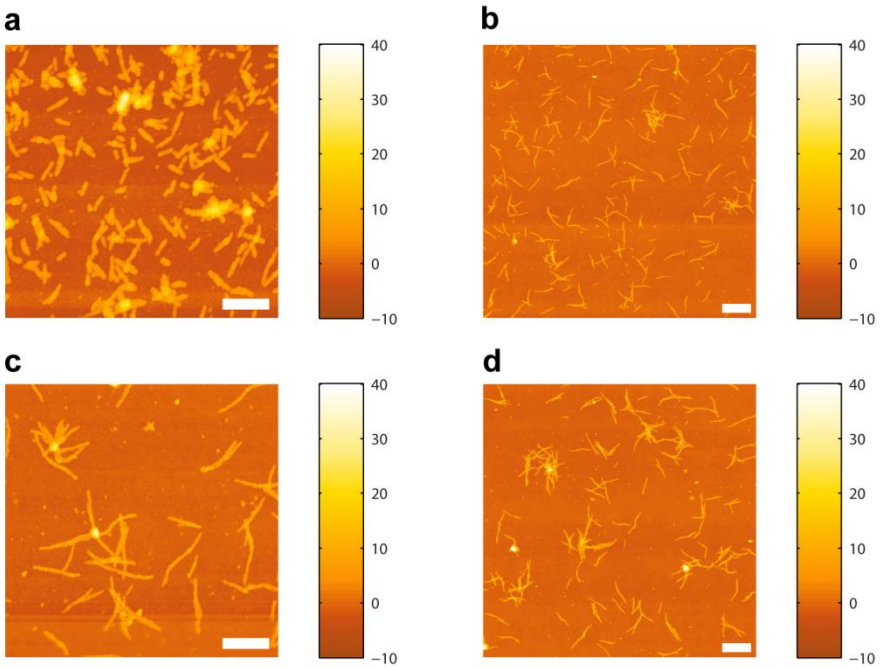

Figure S9. AFM of Htt-ex1 seed growth. a) Htt-ex1-only seeds (undiluted) plus Factor Xa and 4.2 µM Htt-ex1 after 24 hours. The fibers are 50-70 nm wide and ~200 nm in length. Panels b) and d) show Htt-ex1 seed dilutions of 1:5 and 1:10, respectively. Panel c) is an image of the sample in b) at the scale of a) for comparison. The colorbars indicate the z-height in nm. Scale bars a), c) = 500 nm and b), d) = 1 µm.

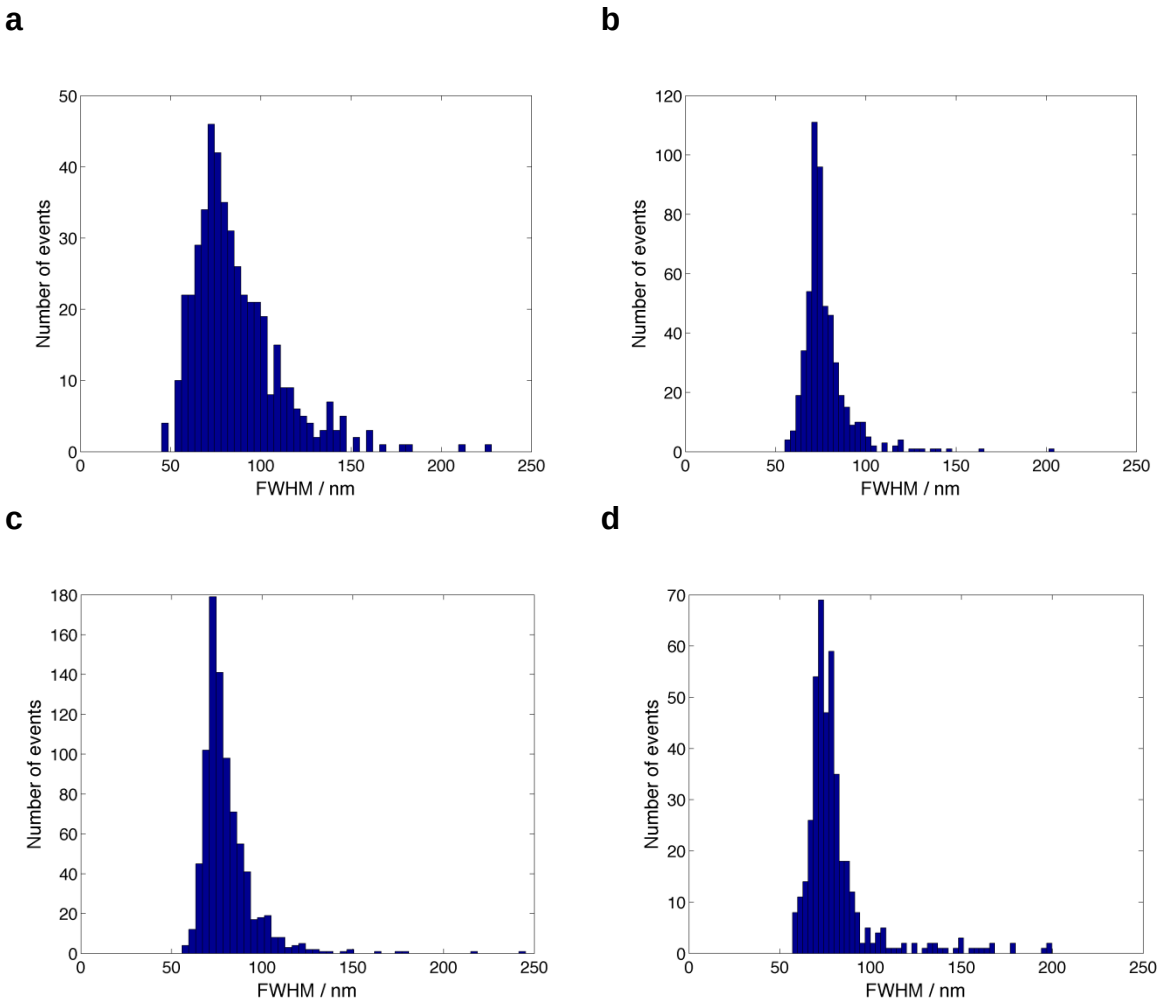

Figure S10. Histograms of sizes of globular species at a) 2, b) 4, c) 8, and d) 24 hours given by the full width at half maximum (FWHM) values of Gaussian fits to the individual species. The statistics of the distributions are given in Table S1.

Table S1. Full width at half maximum (FWHM) values from Gaussian fits to globular species. The SR images analyzed were the larger regions that the panels in Figure 3 were cropped from.

Time (hours)	Mean FWHM (nm)	Standard deviation (nm)	Minimum (nm)	Maximum (nm)	Number of particles
2	86.51	24.60	45.02	227.87	470
4	77.34	13.49	55.12	204.36	537
5	78.45	11.39	60.66	199.84	545
8	80.49	15.51	55.72	245.28	844
16	83.13	20.00	55.54	283.48	597
24	81.24	21.07	56.97	199.72	426
Mean[a]	**81.06**				
Standard deviation[a]	**18.02**				

a. Mean FWHM and standard deviation of all globular species from all time points.

Table S2. FWHM values from Gaussian fits to globular species in two-color SR image (Figure 6d, red species).

SR σ (nm)[a]	Mean FWHM (nm)	Standard deviation (nm)	Minimum (nm)	Maximum (nm)	Number of particles
30	78.07	6.17	70.91	105.01	89
50	122.15	4.83	102.48	139.71	92

a. The value of σ used to plot the Gaussian functions in the SR reconstructions (Figures 3-5 use σ = 30 nm and Figure 6 uses σ = 50 nm). The σ = 30 nm data is presented for comparison with Table S1.

References

1. Dukes, K. D., Rodenberg, C. F., and Lammi, R. K. (2008) Monitoring the earliest amyloid-β oligomers via quantized photobleaching of dye-labeled peptides. *Anal. Biochem. 382*, 29-34.

2. Ding, H., Wong, P. T., Lee, E. L., Gafni, A., and Steel, D. G. (2009) Determination of the oligomer size of amyloidogenic protein beta-amyloid(1-40) by single-molecule spectroscopy. *Biophys. J. 97*, 912-921.

3. Cooper, M., Ebner, A., Briggs, M., Burrows, M., Gardner, N., Richardson, R., and West, R. (2004) Cy3B™: Improving the performance of cyanine dyes. *J. Fluoresc. 14*, 145-150.

4. Jiang, Y., Douglas, N. R., Conley, N. R., Miller, E. J., Frydman, J., and Moerner, W. E. (2011) Sensing cooperativity in ATP hydrolysis for single multisubunit enzymes in solution. *Proc. Natl. Acad. Sci. U. S. A. 108*, 16962-16967.

5. Tam, S., Geller, R., Spiess, C., and Frydman, J. (2006) The chaperonin TRiC controls polyglutamine aggregation and toxicity through subunit-specific interactions. *Nat. Cell Biol. 8*, 1155-1162.

6. Tam, S., Spiess, C., Auyeung, W., Joachimiak, L., Chen, B., Poirier, M. A., and Frydman, J. (2009) The chaperonin TRiC blocks a huntingtin sequence element that promotes the conformational switch to aggregation. *Nat. Struct. Mol. Biol. 16*, 1279-1285.

7. Duim, W. C., Chen, B., Frydman, J., and Moerner, W. E. (2011) Sub-diffraction imaging of huntingtin protein aggregates by fluorescence blink-microscopy and atomic force microscopy. *ChemPhysChem 12*, 2387-2390.

8. Steinhauer, C., Forthmann, C., Vogelsang, J., and Tinnefeld, P. (2008) Superresolution microscopy on the basis of engineered dark states. *J. Am. Chem. Soc. 130*, 16840-16841.

9. Vogelsang, J., Cordes, T., Forthmann, C., Steinhauer, C., and Tinnefeld, P. (2009) Controlling the fluorescence of ordinary oxazine dyes for single-molecule switching and superresolution microscopy. *Proc. Natl. Acad. Sci. U. S. A. 106*, 8107-8112.

10. van de Linde, S., Endesfelder, U., Mukherjee, A., Schuttpelz, M., Wiebusch, G., Wolter, S., Heilemann, M., and Sauer, M. (2009) Multicolor photoswitching microscopy for subdiffraction-resolution fluorescence imaging. *Photochem. Photobiol. Sci. 8*, 465-469.

11. Cordes, T., Strackharn, M., Stahl, S. W., Summerer, W., Steinhauer, C., Forthmann, C., Puchner, E. M., Vogelsang, J., Gaub, H. E., and Tinnefeld, P. (2010) Resolving single-molecule assembled patterns with superresolution blink-microscopy. *Nano Lett. 10*, 645-651.

12. Dempsey, G. T., Bates, M., Kowtoniuk, W. E., Liu, D. R., Tsien, R. Y., and Zhuang, X. (2009) Photoswitching mechanism of cyanine dyes. *J. Am. Chem. Soc. 131*, 18192-18193.

13. Dani, A., Huang, B., Bergan, J., Dulac, C., and Zhuang, X. (2010) Superresolution imaging of chemical synapses in the brain. *Neuron 68*, 843-856.

14. Kaminski Schierle, G. S., van de Linde, S., Erdelyi, M., Esbjorner, E. K., Klein, T., Rees, E., Bertoncini, C. W., Dobson, C. M., Sauer, M., and Kaminski, C. F. (2011) In situ measurements of the formation and morphology of intracellular beta-amyloid fibrils by super-resolution fluorescence imaging. *J. Am. Chem. Soc. 133*, 12902-12905.

15. Lee, H. D., Sahl, S. J., Lew, M. D., and Moerner, W. E. (2012) The double-helix microscope super-resolves extended biological structures by localizing single blinking molecules in three dimensions with nanoscale precision. *Appl. Phys. Lett. 100*, 153701.

16. Dempsey, G. T., Vaughan, J. C., Chen, K. H., Bates, M., and Zhuang, X. (2011) Evaluation of fluorophores for optimal performance in localization-based super-resolution imaging. *Nat. Methods 8*, 1027-1036.

17. Hulko, M., Lupas, A. N., and Martin, J. (2007) Inherent chaperone-like activity of aspartic proteases reveals a distant evolutionary relation to double-psi barrel domains of AAA-ATPases. *Protein Sci. 16*, 644-653.

18. Postis, V. L., Deacon, S. E., Roach, P. C., Wright, G. S., Xia, X., Ingram, J. C., Hadden, J. M., Henderson, P. J., Phillips, S. E., McPherson, M. J., and Baldwin, S. A. (2008) A high-throughput assay of membrane protein stability. *Mol. Membr. Biol. 25*, 617-624.

19. LeVine, H. (1999) Quantification of β-Sheet Amyloid Fibril Structures with Thioflavin T, in *Methods in Enzymology* (R. Wetzel, Ed.) pp 274-284, Academic Press, San Diego, CA.

20. Ferrone, F. (1999) Analysis of Protein Aggregation Kinetics, in *Methods in Enzymology* (Wetzel, R., Ed.) pp 256-274, Academic Press, San Diego, CA.

21. Scherzinger, E., Sittler, A., Schweiger, K., Heiser, V., Lurz, R., Hasenbank, R., Bates, G. P., Lehrach, H., and Wanker, E. E. (1999) Self-assembly of polyglutamine-containing huntingtin fragments into amyloid-like fibrils: Implications for Huntington's disease pathology. *Proc. Natl. Acad. Sci. U. S. A. 96*, 4604-4609.

22. Chen, S., Ferrone, F., and Wetzel, R. (2002) Huntington's disease age-of-onset linked to polyglutamine aggregation nucleation. *Proc. Natl. Acad. Sci. U. S. A. 99*, 11884-11889.

23. Thompson, R. E., Larson, D. R., and Webb, W. W. (2002) Precise nanometer localization analysis for individual fluorescent probes. *Biophys. J. 82*, 2775-2783.

24. Pavani, S. R. P., Thompson, M. A., Biteen, J. S., Lord, S. J., Liu, N., Twieg, R. J., Piestun, R., and Moerner, W. E. (2009) Three-dimensional, single-molecule fluorescence imaging beyond the diffraction limit by using a double-helix point spread function. *Proc. Natl. Acad. Sci. U. S. A. 106*, 2995-2999.

25. Biteen, J. S., Thompson, M. A., Tselentis, N. K., Bowman, G. R., Shapiro, L., and Moerner, W. E. (2008) Super-resolution imaging in live *caulobacter crescentus* cells using photoswitchable EYFP. *Nat. Methods 5*, 947-949.

26. Watkins, L. P., and Yang, H. (2005) Detection of intensity change points in time-resolved single-molecule measurements. *J. Phys. Chem. B. 109*, 617-628.